Journal of Materials Chemistry

Dynamic Article Links

Cite this: J. Mater. Chem., 2012, 22, 25302

www.rsc.org/materials

PAPER

Porosity control and surface sensitivity of titania/silica mesoporous multilayer coatings: applications to optical Bragg resonance tuning and molecular sensing

M. N. Ghazzal,*[a] O. Deparis,[b] A. Errachid,[c] H. Kebaili,[d] P. Simonis,[b] P. Eloy,[a] J. P. Vigneron,[b] J. De Coninck[d] and E. M. Gaigneaux[a]

Received 31st July 2012, Accepted 11th October 2012
DOI: 10.1039/c2jm35107b

Mesoporous dielectric multilayer films exhibit an optical response (Bragg resonance) that is highly sensitive to the chemical environment. Using sol–gel preparation and spin-coating deposition method, titania/silica mesoporous layers were alternatively deposited and consolidated to form a Bragg stack on a glass substrate. Tuning of the effective refractive index of titania layers through the control of their porosity allowed us to tailor the optical response of the multilayer film, and in particular its color, to infiltrate liquids and/or molecules dissolved in a solvent. Selective grafting of hydrophobic molecules on the pore surfaces of titania mesoporous layers was likely to be at the origin of unusual behavior of the Bragg resonance spectral shift and intensity variation. The pore accessibility of the different layers forming the stack was investigated through the infiltration of Rhodamine 6G fluorescent dye. Confocal microscopy revealed a homogeneous distribution of the dye across all the layers of the stack. Capillary attraction induced by adequate pore size distribution between adjacent layers was found to play a key role in liquid infiltration throughout the entire mesoporous dielectric structure.

1. Introduction

Bragg reflectors, also known as one-dimensional (1D) photonic crystals, are dielectric multilayer coating materials having a wide range of optical applications due to their ability to interact with light in a much more complex manner than simple non-structured materials.[1] Interestingly, there are many examples of Bragg reflectors in nature, the most common ones being found in butterfly wings and beetle cuticles.[2] In most of the cases, the biological material (chitin) is porous and derives its physical (structural) colors from 1D photonic crystals made of air/chitin multilayers.[3]

Since the pioneering work of Yablonovitch[4] and John,[5] research related to photonic crystals has been focused on 3D and 2D photonic crystals. Developments of state-of-the-art self-assembly methods for the generation of high-quality opal and inverse opal structures played a crucial role in the study of 3D and 2D photonic crystals.[6] In comparison, 1D photonic crystals received less attention, except in traditional applications such as antireflection coatings or selective optical filters. The development of sol–gel methods, combined with the possibility of fabricating mesoporous films with well defined pore sizes and high optical quality, stimulated renewed interest in 1D photonic crystals, specifically in dielectric mesoporous periodic structures. The latter are typically produced by using spin- or dip-coating processes in which thin mesoporous films[7,8] or nanoparticle films[9,10] of SiO_2 (low refractive index layers) and TiO_2 (high refractive index layers) are alternated. This kind of nano-structured material has potential applications in self-cleaning,[10] lasers[11] and environmental sensing through the infiltration of different types of gases and liquids.[7,8,12] The gas sorption properties of 1D mesoporous photonic crystals are complex and depend on the pore size, the affinity of each type of layer to specific compounds, and the effect of neighboring layers.[13] However, to the best of our knowledge, the issue related to the infiltration of liquids throughout the entire interconnected pore network of multilayer structures has scarcely been investigated.

Herein, we investigate the optical sensing properties of titania/silica mesoporous multilayer films fabricated by a sol–gel method. We propose an alternative approach that allows tuning the refractive index contrast between low- and high-index layers in order to tailor the optical response (Bragg resonance) in the spectral region of interest. More specifically, tuning the effective

[a]*Institute of Condensed Matter and Nanoscience – Molecules, Solids and Reactivity (IMCN/MOST), Université Catholique de Louvain, Croix du Sud 2/17, 1348 Louvain-La-Neuve, Belgium. E-mail: mohamed-nawfal.ghazzal@fundp.ac.be; g_nawfel@yahoo.fr*
[b]*Solid-State Physics Laboratory, Facultés Universitaires Notre-Dame de la Paix (FUNDP), 61 rue de Bruxelles, B-5000 Namur, Belgium*
[c]*Institut des sciences de la vie (ISV) – Université Catholique de Louvain, Croix du sud 4-5/15, B-1348 Louvain-La-Neuve, Belgium*
[d]*Université de Mons – UMONS, Laboratoire de physique des surfaces et interfaces, 20 Place du Parc, 7000 Mons, Belgium*

refractive index of titania layers through the control of their porosity allows us to minimize the number of periods (bilayers) while maximizing the Bragg resonance strength. Our approach contrasts with the one proposed by Sobrado and coworkers for nanoparticle-based 1D photonic crystal films.[14] These authors showed that tuning the layer thicknesses as well as the number of periods allowed modulation of the photonic gap in order to position the Bragg resonance in the targeted spectral region. We also explore the sensitivity of the titania/silica mesoporous multilayer film to the adsorption of liquids. The pore accessibility, the pore filling mechanism and the infiltration of the liquid throughout the whole dielectric mesoporous multilayer structure are discussed.

2. Experimental section

2.1. Material reagents

All the reagents used in this work were of analytical grade and used without any further purification: tetraethyl orthosilicate ($Si(OC_2H_5)_4$), titanium(IV) tetraethoxide ($Ti(OC_2H_5)_4$, 95% Aldrich), ethanol absolute grade, 1-butanol (BuOH) (>99.4%, Alfa Aesar), and hydrochloric acid (Aldrich, 37%); triblock copolymer polyethylene glycol hexadecyl ether (Brij 56, $C_{16}H_{33}(OCH_2CH_2)_nOH$, $n \sim 10$, Aldrich), Pluronic P123 ($M_n \sim 5800$, denoted: $EO_{20}PO_{69}EO_{20}$, Aldrich), Pluronic F127 ($M_n \sim 12\,800$, denoted: $EO_{99}PO_{69}EO_{99}$, Aldrich), 1-hexadecyl trimethylamonium bromide (CTAB, $M_n \sim 364.4$, $(CH_3)_3N(CH_2)_{15}CH_3Br$, Alfa Aesar), dihexadecyl phosphate (DHDP, Aldrich), and tetrahydrofuran (THF). Soda lime glass slides and Indium Tin Oxide (ITO) coated glass slides were purchased from Aldrich. ITO-coated glass slides were used as substrates for ellipsometric measurements.

Mesoporous silica thin films. The procedure was inspired by the study conducted by Grosso *et al.*[15] Briefly, the precursor solutions were prepared by addition of the template to the polymeric sols under acidic conditions. In a typical sol preparation, tetraethyl orthosilicate (TEOS), distilled water, and absolute ethanol were mixed in the molar ratio of 1 : 10 : 10. The pH of the solution was adjusted by adding HCl 37% (pH < 2). The prehydrolysed solution was magnetically stirred at 40 °C for 20 min. Then, an adequate amount of the template was dissolved in absolute ethanol and added to the prehydrolysed solution. Typically, the final molar ratio was 1 TEOS : 20 EtOH : 10 H_2O : 0.1 template. The amount of the added template was chosen so as to produce a film with the desired porosity (see Table 1 for detailed synthesis conditions). The final solution was then aged at 40 °C for 24 h.

Mesoporous titania thin films. The procedure used for the titania film preparation is described in detail elsewhere.[16] During the hydrolysis of the titanium alkoxides, highly acidic conditions were required to prevent an immediate precipitation of TiO_2. Specifically, an adequate amount of titanium(IV) tetraethoxide (TEOT) was dissolved in concentrated hydrochloric acid (37%) at room temperature. After vigorous stirring for 20 min, a hybrid solution was obtained by the addition of the template dissolved in ethanol. The final molar ratio of the solution was 1 TEOT : 2–4 HCl : 9 EtOH : x template. Table 1 summarizes the nature and the specific amount of the template used as a structuring agent for each type of layer. The solutions were subsequently aged under stirring at room temperature for 3 h before the films were spin coated onto soda lime glass (hereafter named SLG) or ITO-coated glass slides.

To build the multilayer dielectric structure, the layers were stacked up step-by-step by spin-coating aqueous solutions of silica or titania sols in air onto the glass substrate for 30 s. Prior to deposition, the substrates were ultrasonically cleaned in detergent, distilled water, acetone, ethanol and finally in distilled water for 15 min each. They were then dried at 150 °C in air. The rotation velocity of the spinner was selected to be 5000 rpm in order to obtain the desired thickness. After the deposition of each layer, the sample was aged in air at room temperature for 12 h, and a subsequent drying was applied following the sequence: 6 hours at 70 °C, 3 hours at 150 °C and 2 hours at 200 °C. The successive consolidation temperatures were selected in order to complete the polycondensation step of the silica or titania framework and to extend the cross-linking between adjacent layers.[8] Calcined films were obtained by heating in air at 400 °C for 2 hours using a temperature rate of 1 °C min^{-1}. These conditions ensured complete removal of organic species and avoided cracks on the films. Finally, the samples were cooled down to room temperature.

2.2. Textural, structural and optical characterizations

Atmospheric ellipsometric porosimetry (AEP) measurements were performed with an AEP instrument from Sopra (Model GES-5E, Sopra, Paris, France) equipped with the software package WinElli2. The AEP characterization technique is the combination of spectral ellipsometry and adsorption porosimetry. The ellipsometric spectral data were fitted in the 1.6–4.5 eV range using a Cauchy-type model in order to determine the film optical constants. Refractive index and film thickness values (at the wavelength of 633 nm) were obtained from a single measurement. For the environmental porosimetric measurements, the ellipsometer was equipped with a variable humidity

Table 1 Composition of film precursor solutions

	Precursor		Composition (mol mol^{-1} metal)						
Sample name	Alkoxide	n (M)	Solvent		H_2O	HCl	Template	n (T)/n (Ti)	Aging temperature
TiP	$Ti(OEt)_4$	0.012	1-Butanol	18	—	4	P123	0.013	25 °C
TiC	$Ti(OEt)_4$	0.012	Ethanol	9	—	2	CTAB	0.1	25 °C
TiB	$Ti(OEt)_4$	0.012	Ethanol	9	—	2	Brij56	0.05	25 °C
TiF	$Ti(OEt)_4$	0.012	Ethanol	9	—	2	F127	0.005	25 °C
SiC	$Si(OC_2H_5)$	0.008	Ethanol	20	10	0.008	CTAB	0.1	40 °C

flow chamber flushed with 2.5 l of air per min. Relative humidity (RH) was adjusted using a mass flow controller and monitored using a RH probe located at the interior of the environmental chamber. Open (*i.e.* accessible) porosity was measured from the change of the optical constants (*n*: refractive index, *k*: extinction coefficient) at atmospheric pressure. Likewise, the film thickness during the water-vapor adsorption/desorption process was measured. The pore size distribution (PSD) was determined from the obtained isotherm *via* a modified Kelvin equation.[17]

Transmission electron microscopy (TEM) analysis was performed using a LEO922 electron microscope operating at 200 keV. The film was scratched off from the substrate, dispersed in ethanol and deposited on copper grids coated with a porous carbon film.

Scanning electron microscopic (SEM) images were taken with a LEO 982 GEMINI microscope equipped with a field emission gun operated with 1 kV as accelerating voltage and 70 μA as emission current. To obtain cross-section images, the SLG slides were broken and placed in the SEM without metallic coating.

Fourier transform infrared (FTIR) spectra were recorded using a Bruker EQUINOX 55 spectrometer. The spectra (for which 200 scans were averaged with a resolution of 4 cm^{-1}) were recorded under static air. FTIR spectra were obtained in the transmittance mode. The spectrum of cleaned SLG slide (without film) was used as a background reference.

Confocal microscopy was performed using a Zeiss LSM 710 apparatus with 63× objective lenses. The confocal microscope was connected to a station equipped with Zen2009 Software as an user interface for image acquisition. To obtain cross-section images, the SLG slides were broken and placed in a cross-section sample holder with the part facing upward and not being directly in contact with the dye solution during soaking. For excitation of the adsorbed Rhodamine 6G molecules, the 488 nm line of an Ar ion laser or, alternatively, the HeNe line at 543 nm was used. A sample was prepared specially for confocal microscopy imaging, consisting of thicker layers of mesoporous oxides for spatial resolution purposes. Each layer was spin-coated at 2000 rpm. The sample was exposed to an ethanolic solution of Rhodamine 6G with a concentration of about 0.003 M for 30 h at 60 °C.

Transmittance measurements in the 300–1100 nm range were carried out using a UV-Vis-NIR spectrophotometer (Cary 5E) at normal incidence angle. Prior to measurements, the samples (multilayer deposited on SLG slides) were washed with ethanol for two hours using Soxhlet.

3. Results and discussion

3.1. TEM analysis

Plane-view TEM images (Fig. 1) give information on the morphology of the mesoporous TiO_2 and SiO_2 films annealed at 400 °C. All the films exhibited mesopores with different structural organizations. Titania and silica films fabricated using Pluronic P123 (TiP) and CTAB (TiC and SiC) as structuring agents did not show structural organization of mesopores, meaning that the critical micellar concentration was not reached in these cases. Indeed, the sol used for the preparation of TiP films was diluted to obtain the thickness required to build the multilayer stack. Although some of the films did not show

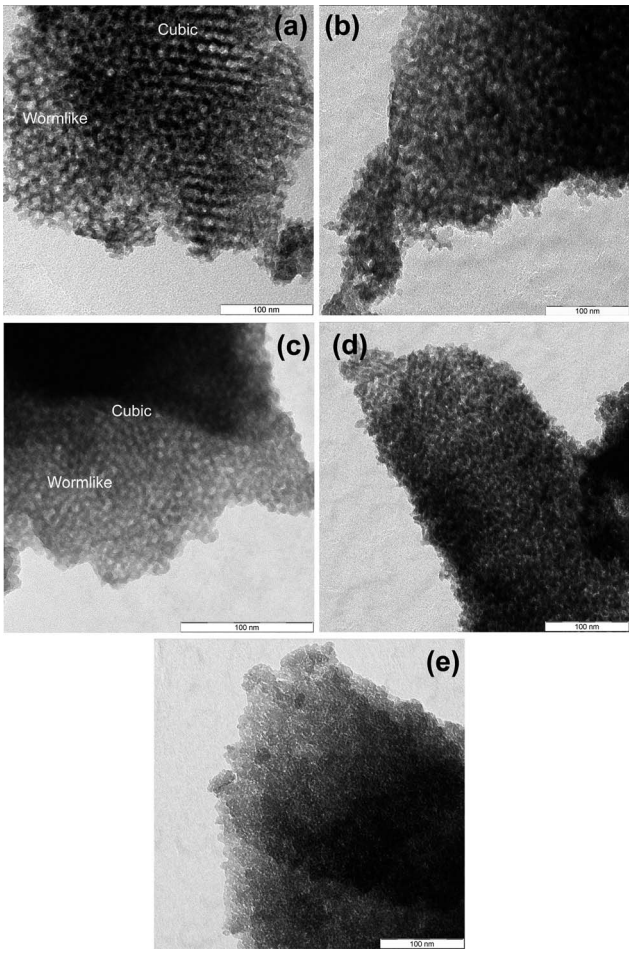

Fig. 1 TEM images of calcined titania (a) TiF, (b) TiP, (c) TiB, (d) TiC and silica and (e) SiC films synthesized with variable template agents.

structural organization of the pores, all the films were porous with pore diameters in the range of 9–11 nm (TiP), 2–4 nm (TiC) and 1–3 nm (SiC). Both TiF and TiB films exhibited regions of different types of structures of mesopores: some of these regions had a well defined ordered (cubic) structure and others had a partly distorted worm-like structure as seen in Fig. 1a (TiF) and c (TiB). The worm-like structure is formed when the inorganic polycondensation is faster than the mesophase formation or results from distortions caused by crystallite growth within the pore walls during the heat treatment.[18,19] Channel walls of 3–4 nm and 2 nm thickness and pore diameters of 7–9 nm and 3–5 nm were estimated for TiF and TiB films, respectively.

3.2. Atmospheric ellipsometric porosimetry

AEP was used to find out how the open porosity, the overall pore size and the effective refractive index could be tuned by changing the template agent. Water vapor was employed as the probe molecule. The effective refractive indexes of porous titania and silica layers at $\lambda = 633$ nm were determined under dry atmosphere (pores filled by air). They were found to be in the range of 1.52–1.74 for titania films and 1.26 for the silica film (Table 2). These low values (compared to 2.18 (ref. 16) and 1.44 (ref. 20) for dense titania and silica films) were due to the porosity left by the

Table 2 Optical and textural characteristics (spherical pore model) obtained by atmospheric ellipsoporosimetric porosimetry and TEM analysis for the sol–gel thin films

Sample Name	Thickness (nm)	Porosity (%)	Refractive index	Av pores[a] (nm) (TEM)	Av pores[a] (nm) (adsorption)	fwhm (nm) (adsorption)
TiP	114	40.7	1.52	9–11	14	3
TiF	128	32.6	1.59	7–9	8	2.5
TiC	90	28.4	1.65	2–4	4	1.2
TiB	80	20.1	1.74	3–4	4.5	2
SiC	97	45.6	1.26	1–3	3	0.4

[a] Diameter.

template agent after calcination. The pore size distribution (PSD) was deduced from Kelvin's equation by employing the water contact angle values measured after the films were ultrasonicated under ethanol ($\theta \approx 10°$). PSDs for all films are shown in Fig. 2. In Table 2, pore diameter values (extracted from PSDs) are reported: diameters ranged from 4 to 14 nm in titania films (depending on the template) and it was about 3 nm in the silica film. The width of the pore size dispersion was in the range of 1.2–3 nm for titania films (Fig. 2a) whereas dispersion was very small (<0.5 nm) for the silica film (Fig. 2b). Pore diameter values obtained by AEP were in fair agreement with those estimated from TEM analysis and they corresponded to those reported by other groups.[15,17]

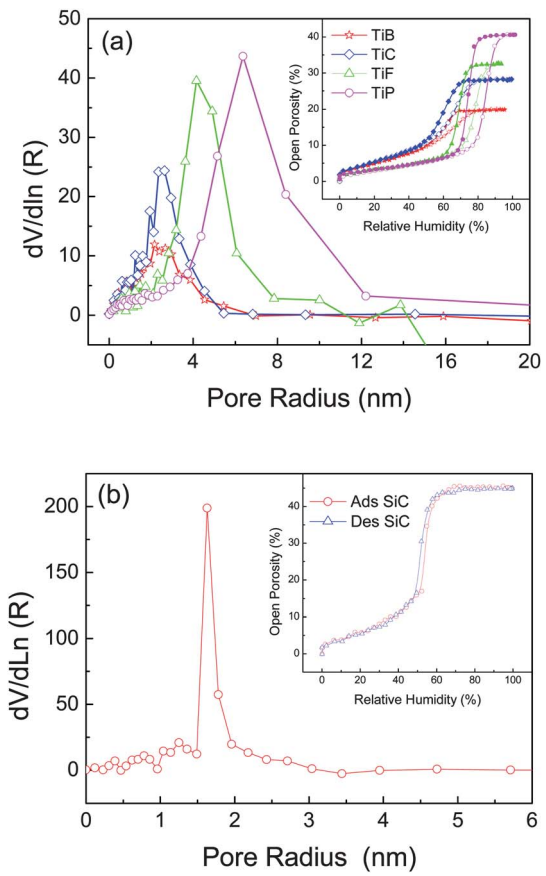

Fig. 2 Pore size distribution calculated using a modified Kelvin equation for TiF, TiP, TiB, TiC (a) and SiC (b) films. Insets: water adsorption/desorption isotherms for titania (a) and silica (b) films.

Isotherms of water adsorption–desorption are shown as insets in Fig. 2 for titania and silica films. The Bruggeman Effective Medium Approximation (BEMA) is commonly used to corroborate the porosity value deduced from water adsorption isotherms, assuming that all pores are accessible and filled with water.[18] All adsorption isotherms showed, at low RH values, a slight increase of the porosity as a function of relative humidity (RH), meaning that the micropores present on titania or silica walls were first filled with water.[21] At higher RH values, the mesopores themselves became filled with water *via* capillary condensation, which resulted in the sudden increase of the porosity (*i.e.* amount of adsorbed water) as a function of RH. The isotherms of titania films exhibiting different pore size distributions showed that the capillary pressure of water condensation, corresponding to the complete filling of the mesopores, became higher as the pore size increased (inset Fig. 2a). The reversible IV-adsorption/desorption isotherm type with a characteristic hysteresis loop in the cases of TiP and TiF films suggested that the pores had a cylindrical shape and were open at each extremity.[16] The slope of the adsorption/desorption branches of the isotherms at high RH was steeper in the SiO_2 film than in TiO_2 films. This behavior was due to a narrower pore size distribution in the SiO_2 film, with a mean pore radius of 1.6 nm, a value that agreed very well with the expected pore size of the CTAB template mesoporous SiO_2.[15] The low value of the effective refractive index measured under dry conditions (n_{633nm} = 1.26) was characteristic of the presence of a large fraction of pores, up to 45%, within the silica film (Table 2 and inset of Fig. 2a). The maximal open porosity in titania films was measured to be 41% for TiP films, whereas it was only 20% for TiB films (Table 2 and inset of Fig. 2a).

3.3. Optical properties of mesoporous dielectric structure

The SEM image of the cross-section of a mesoporous multilayer stack built by alternating layers of SiC and TiF three times (3 bilayers) is shown in Fig. 3a. The layers appeared to be uniform over the cross-section and crack free. Thanks to the repeated coating/polycondensation/calcination steps and to the slow temperature rate applied during heating (1 °C min^{-1}), we did not observe any mixed phase at the interface of the layers. The layers were well distinguishable on the cross-section SEM image because of the difference in the density of the materials (higher density for TiO_2 than SiO_2: darker layers on the SEM image are SiO_2 layers which alternate with brighter TiO_2 layers).

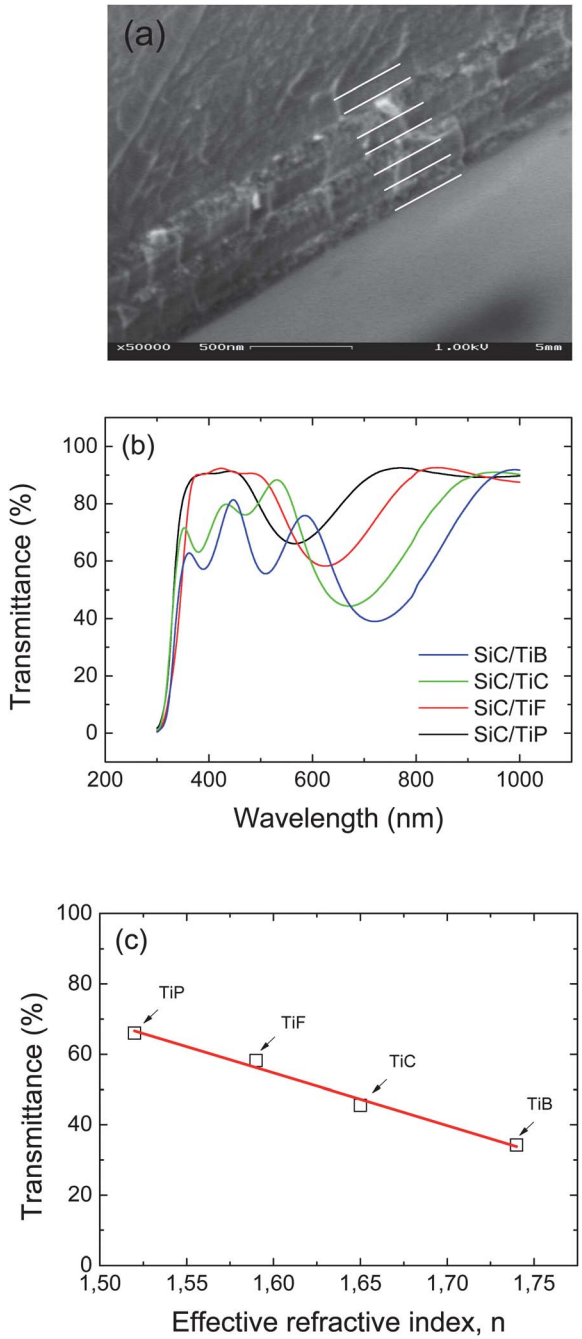

Fig. 3 (a) SEM image of the cross-section of mesoporous multilayer consisting of three alternating layers of SiC and TiF. (b) Transmittance spectra of mesoporous titania/silica Bragg stacks (three bilayers), for which the porosity in titania layers is different. (c) Transmittance values at Bragg resonance as a function of the effective refractive index of the titania layers.

The optical responses (transmittance spectra) of mesoporous SiO_2/TiO_2 Bragg stacks are shown in Fig. 3b. In all cases, the transmittance exhibited a dip (main lobe of the Bragg resonance) in the visible-NIR region. Secondary lobes (on the short-wavelength side of the main lobe) were detectable for SiC/TiB and SiC/TiC samples. They are known to arise from the interference of light waves partially reflected and transmitted at the top and bottom surfaces of the multilayer stack. Differences in the Bragg peak intensity (*i.e.* height of the transmittance dip) were observed between samples. The intensity decreased as the porosity of TiO_2 layers (see Table 2) increased. A good correlation was found between the effective refractive index of TiO_2 layers (see Table 2) and the transmittance minimum value (Fig. 3c), highlighting the direct relationship between the porosity and the optical response. The (effective) refractive index of each TiO_2 layer of the multilayer stack was tuned by controlling the concentration and the type of surfactant added to the sol composition. As the porosity was increased, the refractive index of the mesoporous TiO_2 layers decreased (in the following order, see Table 2: $n_{TiB} > n_{TiC} > n_{TiF} > n_{TiP}$). Therefore, the refractive index contrast between both types of layers was reduced and the Bragg peak intensity decreased. The first-order Bragg wavelength (position of the main lobe) was sensitive to the change of the refractive index as well. According to the Bragg law,[22] the position of the (first-order) Bragg peak is related to the refractive index and thicknesses of both layers forming the periodic structure:

$$\lambda = 2(n_{TiO_2}d_{TiO_2} + n_{SiO_2}d_{SiO_2}) \quad (1)$$

where λ is the first-order Bragg wavelength, n and d are the refractive index and thickness of the mesoporous TiO_2 and SiO_2 layers, respectively. Eqn (1) predicts that the Bragg wavelength is blue-shifted (*i.e.* moves to shorter wavelengths) as the refractive index of one of the two layers decreases. This prediction was verified in our samples since the transmittance dip was blue-shifted for decreasing values of the titania refractive index, *i.e.* according to the sequence: TiB, TiC, TiF and TiP (Fig. 3b). The spectral position and the height of the transmittance dip could be tuned across the visible and near infra-red ranges by solely modifying the refractive index of the mesoporous TiO_2 layer. The high contrast between SiO_2 and TiO_2 refractive indexes allowed obtaining as high as 60% reflection (40% transmission) of the incident light (at 700 nm wavelength) with only three periods (*cf.* SiC/TiB multilayer stack).

The intensity of the Bragg peak could be further tuned by varying the number of layers in the stack (Fig. 4). The most intense Bragg peak (90% reflectance, 10% transmittance) was achieved with a stack of ten SiC/TiF bilayers.

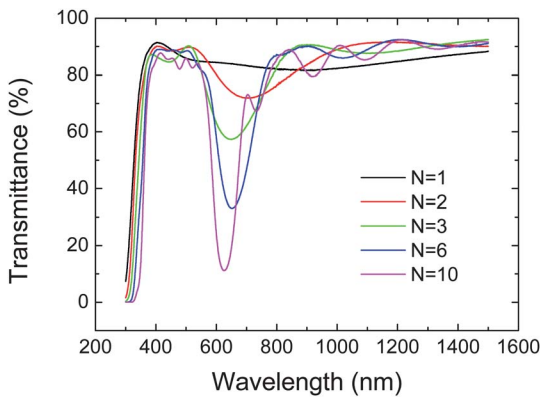

Fig. 4 Transmittance spectra of mesoporous SiC/TiF stacks of different numbers of bilayers (from 1 to 10).

3.4. Sensitivity of the mesoporous multilayer to the environment

3.4.1. Pore accessibility. In order to check the accessibility of the pores to molecules from the environment a 3×SiC/TiF mesoporous multilayer was exposed to a Rhodamine 6G (Rh6G) dye solution. The distribution of the dye fluorescence in the sample cross-section which was not exposed directly to the Rh6G solution was explored using confocal microscopy at two different excitation wavelengths (488 nm and 543 nm) responsible for green and red fluorescences, respectively. The transmittance of the multilayer (at normal incidence) after Rh6G infiltration is shown in Fig. 5a. The Bragg peak is located at the near-infrared region (1123 nm) for that sample. Indeed, the thickness of each layer was increased (compared with other samples) by reducing the spinning speed (2000 rpm instead of 5000 rpm) in order to improve the spatial resolution of the layers in confocal microscopy. The secondary transmittance dip at 526 nm was associated with the Rh6G absorption band (530 nm (ref. 16)) but it also coincided with the second order Bragg resonance (therefore both absorption and reflection were responsible for that transmittance minimum). Imaging of both red and green fluorescence in the cross-section (images superimposed in Fig. 5b) suggested that the Rh6G molecules were distributed across the entire mesoporous multilayer structure. Indeed, the alternating TiF and SiC layers were clearly distinguishable on fluorescence images and their visibility was enhanced by the shift of the fluorescence emission spectrum of Rh6G molecules as a function of the dielectric environment (TiF or SiC). The fluorescence emission intensities along the cross-section (dashed line in Fig. 5b) are shown in Fig. 5c. The red and green curves, corresponding to different fluorescence emission wavelengths, exhibited local maxima associated with aggregation of the dye into each layer. The fluorescence emission shift can either be attributed to the interaction of the cationic dye molecules with different host environments (Si–O^- or Ti–O^-) (from one layer to another) or to an aggregation form of the dye.[23,24] Despite the interaction of Rh6G molecules with the oxide layer materials, the dye penetrated through the top surface and diffused from the edges and eventually reached all the layers. Therefore, we conclude that the entire available pore surface of the mesoporous multilayer was accessible.

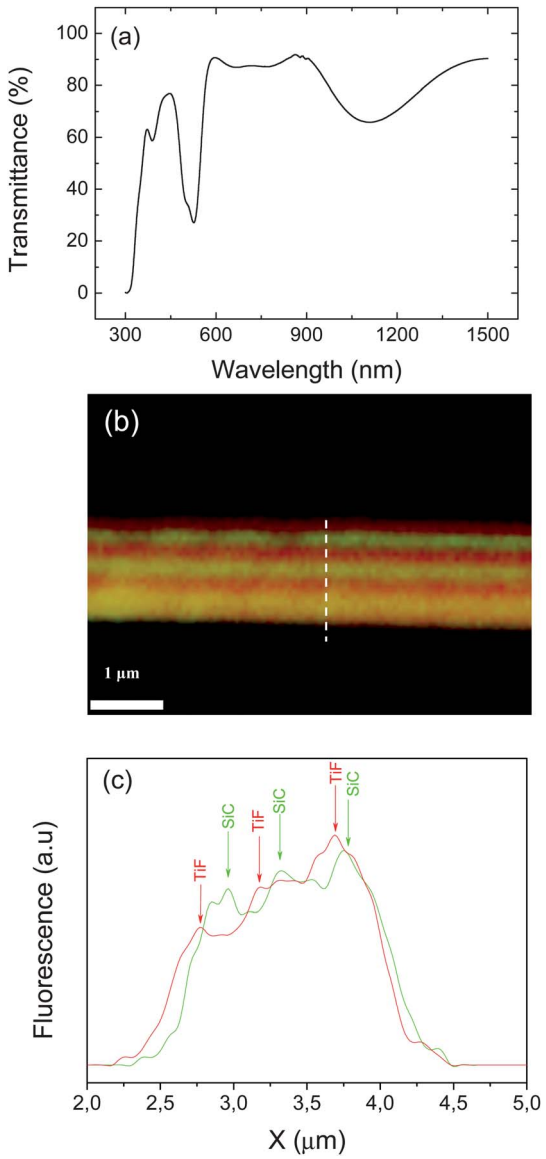

Fig. 5 (a) Transmittance spectrum of the Rh6G-infiltrated 3×SiC/TiF sample. (b) Confocal microscopy image of the cross-section of the Rh6G-infiltrated stack: the image is the superposition of two images of the red and green fluorescence, respectively. (c) Fluorescence profiles measured along the dashed line on the image (b), red and green curves correspond to fluorescence excited at 488 nm and 543 nm, respectively. The (mean) positions of the TiF and SiC layers in the stack are marked by arrows.

3.4.2. Pore filling and capillary attraction of the liquid. Filling of the pores of the mesoporous multilayer structure in a liquid medium is an important issue for sensing applications. The optical response of the multilayer indeed is affected by the fraction of pores and the number of layers which are filled by the target molecules. Colodrero and co workers[9] revealed that filling the pores of nanoparticle-based 1D photonic crystals by water vapor was affected by a different pore size in one type of layers and could be influenced by the pore size of adjacent layers. When a mesoporous multilayer is immersed in a liquid medium, capillary attraction, which implies molecule transport through the pore network, can influence the filling of the pores and hence the optical response used for sensing. In order to study the capillary attraction due to the difference in pore sizes between SiO_2 and TiO_2 layers, two mesoporous multilayers were selected. The first one (3×SiC/TiF) was composed of smaller pores in SiC layers (diameter $d = 3$ nm) and larger pores in TiF layers ($d =$ 8 nm), whereas the second one (3×SiC/TiB) had equal average pore size diameters in both layers ($d \approx$ 3–4.5 nm). The evolution of their optical response, recorded at different times during soaking in water, is shown in Fig. 6a and 6b, respectively. The corresponding changes in the Bragg peak transmittance intensity and wavelength (relative to their values before soaking) are plotted in Fig. 6c and 6d, respectively. In each case, an abrupt red shift and a variation of the intensity of the Bragg peak were observed. After only one minute of soaking, differences in the registered trends (relative intensity and wavelength) were already found between the two samples. For the 3×SiC/TiF multilayer, the relative transmittance intensity increased slightly for a while

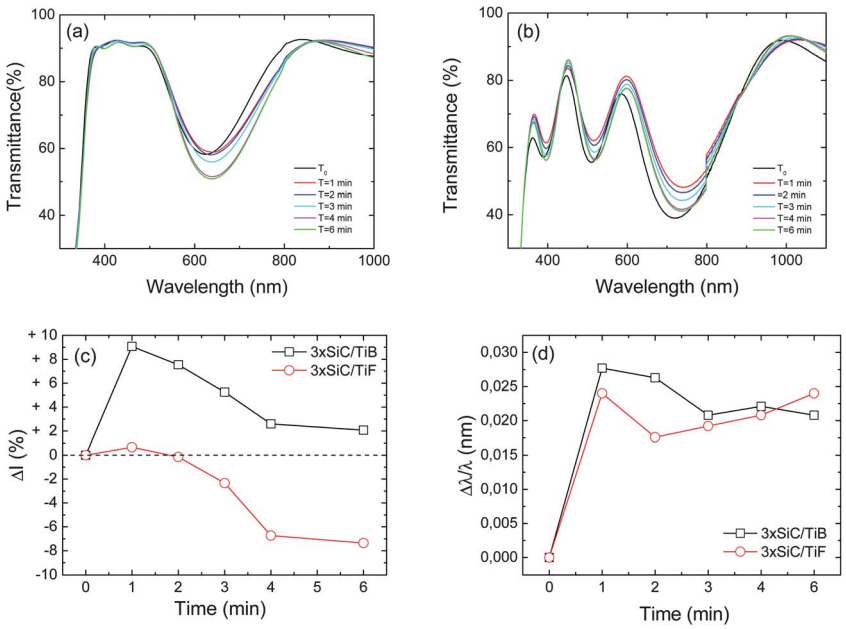

Fig. 6 Evolution of transmittance spectra of (a) 3×SiC/SiF and (b) 3×SiC/TiB samples at different times t during soaking in water ($t = 0$ is before soaking, *i.e.* dry conditions). Evolution of the relative (with respect to $t = 0$) (c) intensity ΔI (the difference of the Bragg peak strength) and (d) spectral position $\Delta\lambda/\lambda$ of the Bragg resonance (main transmittance dip) as function of time during soaking in water.

then decreased and finally saturated to a lower value, whereas for the 3×SiC/TiB multilayer it first increased suddenly and then tended to recover its initial value. For both samples, changes in the Bragg peak intensity (related to refractive index contrast) were accompanied by changes in the Bragg peak position (related to average refractive index). Considerations on pore size differences between layers suggest that water infiltration occurs in the 3×SiC/TiF multilayer, resulting in a gradual filling of the pores of all the layers, whereas the liquid cannot infiltrate the pores of the 3×SiC/TiB multilayer. The reason for the infiltration of the pores of the 3×SiC/TiF multilayer is the capillary attraction of the liquid due to the difference in pore sizes between adjacent layers. In contrast, pore sizes are identical in all layers of 3×SiC/TiB multilayer which results in the absence of the capillary attraction and therefore the absence of pore filling in that sample. In this situation, however, for the change of the Bragg resonance observed during the soaking experiment another explanation needs to be found. Our assumption is that water adsorbed at the outer surface of the multilayer formed a thin film which could be responsible for the observed red shift and the Bragg peak intensity reduction (increase of relative transmittance) in the non-infiltrated 3×SiC/TiB multilayer. Finally, the evaporation of the water thin film from the outer surface could explain the long term evolution of the Bragg peak intensity, which eventually returned to its value before soaking.

3.4.3. Sensing ability. The optical response of a 10×SiC/TiF mesoporous multilayer coating before and after soaking in water is shown in Fig. 7a. The SEM image (Fig. 7b) shows, in cross-section, the 10 bilayers of SiC and TiF prepared by spin-coating. The coating appeared to be of high optical quality and crack free thanks to the soft calcination steps. After soaking in water, increase of the Bragg peak intensity (*i.e.* decrease of the transmittance intensity), red-shift and broadening of the Bragg peak (FHWM) were observed. These spectral modifications were significant enough to result in a perceptible color change of the coating, from green (before water soaking) to orange-red (after water soaking). As expected from the Bragg law (eqn (1)), the modification of the optical response (hence the color) is induced

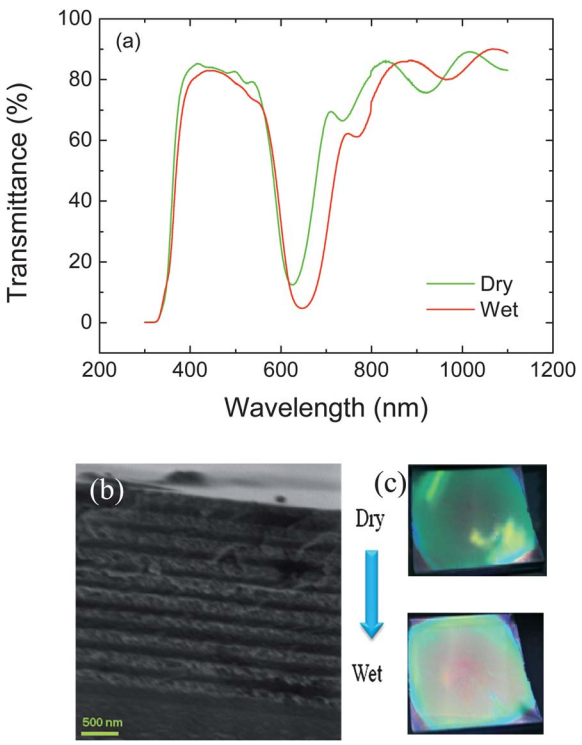

Fig. 7 (a) Transmittance spectra of 10×SiC/TiF sample in dry and wet conditions. (b) SEM image of the cross-section showing the ten SiC/TiF bilayers. (c) Photographs of the sample in dry and wet conditions.

by changing the effective refractive index of the mesoporous multilayer structure due to water infiltration.[7,25]

The dielectric mesoporous multilayer structure is able to trap not only a pure liquid compound, such as water, into its pore network but also a solid compound dissolved in solution. The optical response of a 3×SiC/TiF mesoporous multilayer coating before and after soaking in a solution of THF containing dissolved DHDP is shown in Fig. 8a. The sample was immersed into a continuously stirred 0.01 mol l^{-1} solution of DHDP dissolved in THF. Filling the pores of the multilayer structure caused an increase of the effective refractive index, leading to a red-shift (~50 nm) and a broadening of the transmittance dip (Fig. 8a, red curve). As the Bragg peak moved from the visible region (400–700 nm) to the NIR region (>700 nm), the coating became almost totally transparent after DHDP post-grafting (inset Fig. 8a).

The efficiency of grafting the DHDP molecules into the mesoporous multilayer structure was evaluated by washing of the sample using the Soxhlet procedure. After washing with THF for one hour, a blue shift of the transmittance dip was observed (Fig. 8a, blue curve). However, the initial position of the Bragg peak (Fig. 8a, black curve) was not recovered after washing, which means that DHDP molecules remained strongly linked to the pore surface of the mesoporous multilayer. A comparison of DHDP desorption from different metal oxide films grown on SLG substrates can be done (Fig. 8b). Typically, non-porous (template free) TiO_2, mesoporous SiC, mesoporous TiF and 3×SiC/TiF samples were exposed to a solution containing DHDP until adsorption equilibrium was reached. Subsequently, the samples were washed with THF and leaching of DHDP was monitored by measuring the integrated IR absorbance of the C–H band in the 2700–3000 cm^{-1} region. After washing with THF, the concentration of DHDP molecules adsorbed by a non-porous TiO_2 film and mesoporous SiC film dropped down rapidly to zero. In comparison with the non-porous TiO_2 film, more DHDP molecules remained anchored to the mesoporous TiF film. For the mesoporous silica film, the result suggests that DHDP molecules diffuse into the pore network and are adsorbed on silica pore surfaces by weak bonds. For the 3×SiC/TiF mesoporous multilayer film, the (initial) concentration of adsorbed DHDP molecules was three times higher than that in the mesoporous TiF film. This result suggests that DHDP molecules diffuse through all layers of the multilayer structure and are strongly bound to TiF pore surfaces, in agreement with previous works.[26,27] The fact that strong bonding occurs in the titania mesopores explains the impossibility to recover the initial position of the Bragg peak.

The red-shift of the Bragg peak ($\Delta\lambda$) was measured after exposition of the 3×SiC/TiF film to different adsorbents including dissolved solid compounds (DHDP molecules in THF solvent), hydrophilic molecules (H_2O) and hydrophobic molecules (C_6H_{14}, *n*-hexane). The measured shift was equal to: $\Delta\lambda$ = 47 nm (DHDP), 15 nm (water) and 11 nm (hexane). No correlation between the refractive index of the compounds (n_{H_2O} = 1.333 and n_{hexane} = 1.375) and $\Delta\lambda$ was observed, in contrast to what was reported in other studies.[28] Indeed, in spite of the higher refractive index of hexane as compared with that of water, $\Delta\lambda$ was smaller for hexane than for water. This result suggests that the interaction between the molecules and the mesoporous metal oxide surface influenced the infiltration behavior of the compound through the dielectric mesoporous multilayer structure. Such a dissimilar response (hexane *versus* water) cannot be attributed to the refractive index difference between both substances (the higher refractive index of hexane *versus* water should lead to a larger red-shift of the Bragg peak whereas it is the opposite that is observed), but rather to a difference in the affinity of the pore walls for the different adsorbed species. Our

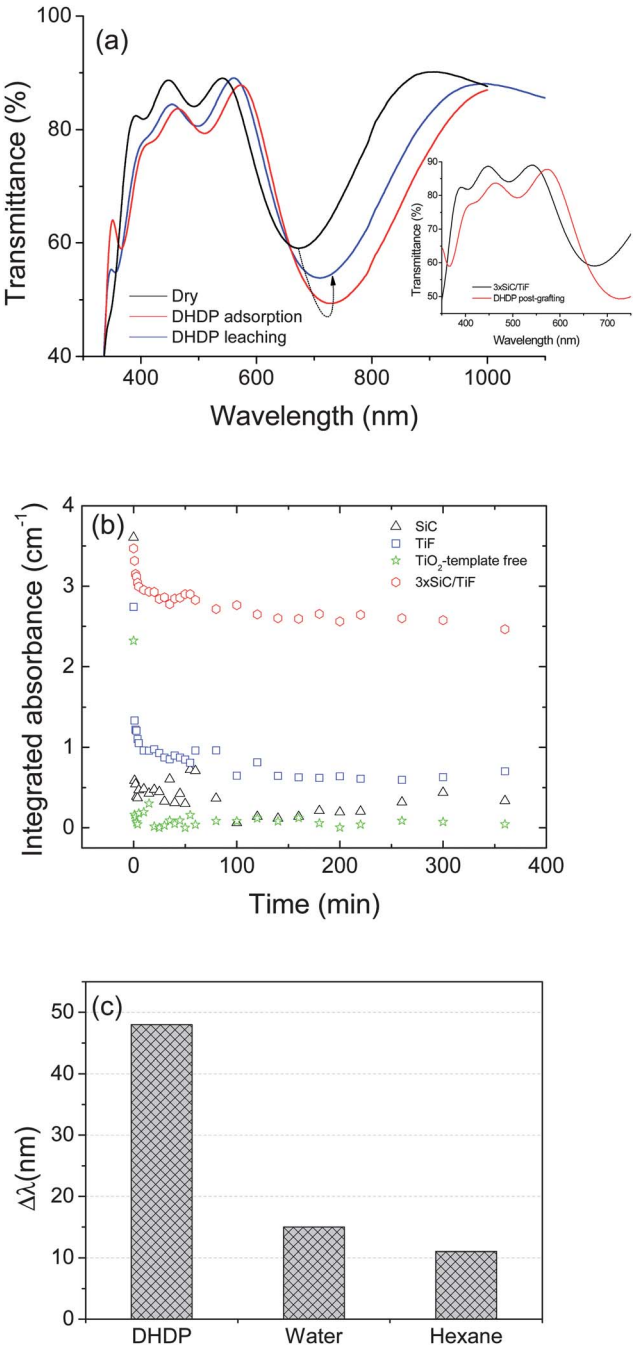

Fig. 8 (a) Transmittance spectra of 3×SiC/TiF in air, after DHDP adsorption and after Soxley washing. (b) Leaching out of DHDP for TiO_2-template free, SiC, TiF and 3×SiC/TiF multilayer. DHDP is previously adsorbed for 6 h. The absorbance values correspond to IR bands integrated between 2700 and 3000 cm^{-1}. (c) Bar graph showing the $\Delta\lambda$ obtained for 3×SiC/TF after DHDP adsorption and the exposition of different environments.

results confirm previously reported observation on the affinity of mesoporous surface to external molecules having different polarities. Indeed, Fuertes *et al.*[8] showed that turning a mesoporous TiO_2 surface hydrophobic by post-grafting can be a way of tailoring its affinity for different molecules. Choi *et al.*[7] revealed that the selectivity and sensitivity of mesoporous Bragg stacks were highly dependent on the pore surface properties of the mesoporous metal oxide layers and on their adsorption affinity for the molecules of interest.

4. Conclusion

We demonstrated that the control of the porosity of titania layers within a titania/silica mesoporous multilayer Bragg stack allowed tailoring the strength (intensity) and the position (wavelength) of the Bragg resonance appearing in the optical transmittance spectrum. As a result, the multilayer coating was made highly transmitting or reflecting in selected regions of the electromagnetic spectrum. The main advantage of our approach was the opportunity of using a reduced number of bilayers in the stack while keeping a strong Bragg resonance through a suitably controlled refractive index contrast. The open porosity present in each layer of the stack enabled absorption of liquids and solid molecules dissolved in an appropriate solvent. We showed that the difference in pore size distributions between adjacent layers was a limiting parameter for liquid infiltration throughout the mesoporous multilayer structure. A suitable distribution of the porosities in the multilayer stack induced a capillary effect which was responsible for efficient filling of the pores throughout the multilayer.

Acknowledgements

Researchers are grateful to the "Région Wallonne" (Belgium) for its financial support.

References

1 J. Ge and Y. Yin, *Angew. Chem., Int. Ed.*, 2011, **50**, 1492.
2 J. P. Vigneron, M. Rassart, C. Vandenbem, V. Lousse, O. Deparis, L. P. Biró, D. Dedouaire, A. Cornet and P. Defrance, *Phys. Rev. Lett.*, 2006, **73**, 041905.
3 S. Kinoshita, *Structural Colors in the Realm of Nature*, World Scientific Publishing Co, Singapore, 2008.
4 E. Yablonovitch, *Phys. Rev. Lett.*, 1987, **58**, 2059.
5 S. John, *Phys. Rev. Lett.*, 1987, **58**, 2486.
6 C. I. Aguirre, E. Reguera and A. Stein, *Adv. Funct. Mater.*, 2010, **20**, 2565.
7 S. Y. Choi, M. Mamak, G. V. Freymann, N. Chopra and G. A. Ozin, *Nano Lett.*, 2006, **6**, 2456.
8 M. C. Fuertes, F. J. López-Alcaraz, M. C. Marchi, H. E. Troiani, V. Luca, H. Míguez and G. J. Soler-Illia, *Adv. Funct. Mater.*, 2007, **17**, 1247.
9 S. Colodrero, M. Ocana, A. R. Gonzalez-Elipe and H. Miguez, *Langmuir*, 2008, **4**, 9135.
10 Z. Wu, D. Lee, M. F. Rubner and R. E. Cohen, *Small*, 2007, **3**, 1445.
11 D. P. Puzzo, F. Scotognella, M. Zavelani-Rossi, M. Sebastian, A. J. Lough, I. Manners, G. Lanzani, R. Tubino and G. A. Ozin, *Nano Lett.*, 2009, **9**, 4273.
12 B. V. Lotsch and G. A. Ozin, *Adv. Mater.*, 2008, **20**, 4079.
13 M. C. Fuertes, S. Colodrero, G. Lozano, A. R. Gonzalez-Elipe, D. Grosso, C. Boissiere, C. Sanchez, G. J. de, A. A. Soler-Illia and H. MIguez, *J. Phys. Chem. C*, 2008, **112**, 3157.
14 O. Sanchez-Sobrado, M. E. Calvo and H. Miguez, *J. Mater. Chem.*, 2010, **20**, 8240.
15 D. Grosso, A. R. Balkenende, P. A. Albouy, M. Lavergne, L. Mazerollese and F. Babonneau, *J. Mater. Chem.*, 2000, **10**, 2085.
16 M. N. Ghazzal, H. Kebaili, M. Joseph, P. Eloy, J. De Coninck and E. M. Gaigneaux, *Appl. Catal., B*, 2012, **115**, 276.
17 C. Boissiere, D. Grosso, S. Lepoutre, L. Nicole, A. B. Bruneau and C. Sanchez, *Langmuir*, 2005, **21**, 12362.
18 J. H. Panab and W. I. Lee, *New J. Chem.*, 2005, **29**, 841.
19 E. L. Crepaldi, G. J. Soler-Illia, D. Grosso, F. Cagnol, F. Ribot and C. Sanchez, *J. Am. Chem. Soc.*, 2003, **125**, 9770.
20 A. Vincent, S. Babu, E. Brinley, A. Karakoti, S. Deshpande and S. Sea, *J. Phys. Chem. C*, 2007, **111**, 8291.
21 M. I. Clerc, P. Davidson and A. Davidson, *J. Am. Chem. Soc.*, 2000, **122**, 11925.
22 T. Alfrey Jr, E. F. Gurnee and W. Schrenk, *Polym. Eng. Sci.*, 1969, **9**, 400.
23 M. J. Tapia, F. L. Arbeloa, T. L. Arbeloa, I. L. Arbeloa and R. A. Schoonheydt, *Clay Miner.*, 1994, **29**, 105.
24 B. J. Scott, G. Wirnsberger and G. D. Stucky, *Chem. Mater.*, 2001, **13**, 3140.
25 B. V. Lotsch and G. A. Ozin, *ACS Nano*, 2008, **2**, 2065.
26 P. C. Angelomé and G. J. A. A. Soller-Illia, *Chem. Mater.*, 2005, **17**, 322.
27 P. C. Angelomé, M. C. Fuertes and G. J. A. A. Soller-Illia, *Adv. Mater.*, 2006, **18**, 2397.
28 S. Colodrero, M. Ocan and H. Miguez, *Langmuir*, 2008, **24**, 4430.

